Applied Energy 254 (2019) 113726

Contents lists available at ScienceDirect

Applied Energy

journal homepage: www.elsevier.com/locate/apenergy

A novel resistor-inductor network-based equivalent circuit model of lithium-ion batteries under constant-voltage charging condition

Jufeng Yang[a], Yingfeng Cai[a], Chaofeng Pan[a], Chris Mi[b,*]

[a] Automotive Engineering Research Institute, Jiangsu University, 301 Xuefu Road, Zhenjiang, Jiangsu 212013, China
[b] Department of Electrical and Computer Engineering, San Diego State University, 5500 Campanile Drive, San Diego, CA 92182, USA

HIGHLIGHTS

- Introduced a novel RL network-based ECM to describe the battery CV charging current.
- Developed enhanced ECMs containing multiple parallel-connected RL networks.
- Conducted a comparative study to determine the preferred model structure.
- Proposed a simplified model with satisfactory current estimation accuracy.
- Validated the feasibility and superiority with test data after different cycles.

GRAPHICAL ABSTRACT

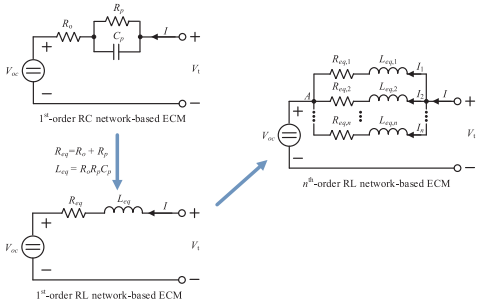

ARTICLE INFO

Keywords:
Lithium-ion battery
Electric vehicles (EVs)
Constant-voltage (CV) charge
Equivalent circuit model (ECM)
Resistor-inductor (RL) network

ABSTRACT

A constant-current constant-voltage (CCCV) charge protocol is commonly used for lithium-ion batteries. The dynamic characteristic of the constant-voltage (CV) charging current is discovered to be related to battery aging. In order to quantitatively describe the load current during the CV charging period, an equivalent circuit model (ECM) based on the resistor-inductor (RL) network is proposed in this paper. Motivated by the current expression derived based on the conventional resistor–capacitor (RC) network-based ECM, an RL network-based ECM is developed to characterize the CV charging current. Then, the parallel-connected RL networks are employed to improve the model fidelity. The test data of four lithium iron phosphate ($LiFePO_4$) batteries in different aging states are employed to validate the proposed model. Comparative results show that the proposed 2nd-order ECM is the best choice, considering both the model accuracy and complexity. In addition, a simplified 2nd-order model is proposed, achieving a satisfactory accuracy with only three model parameters to be identified. Therefore, this model can be easily implemented in the battery management system (BMS).

1. Introduction

The transportation system is developing towards the electrification [1,2] and intelligence [3,4]. The success of vehicle electrification depends on the low-cost, safe and efficient on-board battery pack. Recently, lithium-ion batteries have been widely used in electric vehicles (EVs) due to their advantages of the long cycle life, high energy and power capabilities [5,6]. In order to ensure the safe and efficient operation, a sophisticated battery management system (BMS) is required to monitor and control the battery parameters such as voltage, current, state-of-charge (SoC) [7,8], state-of-health (SoH) [9,10], state-of-energy (SoE) [11] and so on, in real time. In the battery management

* Corresponding author.
E-mail address: cmi@sdsu.edu (C. Mi).

https://doi.org/10.1016/j.apenergy.2019.113726
Received 7 May 2019; Received in revised form 24 July 2019; Accepted 9 August 2019

Nomenclature

Abbreviations

BMS	battery management system
CCCV	constant-current constant-voltage
CC	constant-current
CV	constant-voltage
ECM	equivalent circuit model
EV	electric vehicle
HPPC	hybrid pulse power characterization
$LiFePO_4$	lithium iron phosphate
OCV and V_{oc}	open circuit voltage
RC	resistor-capacitor
RL	resistor-inductor
RMSE	root mean-squared error
SoC	state-of-charge
SoH	state-of-health
A, B and C	function coefficients
C_p, R_p	capacitance and resistance in the RC network
I	load current
I_k	branch current through each RL network
$I_{mea,i}$	measured current
$I_{est,i}$	estimated current
L_{eq}	equivalent inductance
n	order of the model
N	recorded data size
NLS	nonlinear least squares
R^2	R-square
R_o	ohmic resistance
R_{eq}	equivalent resistance
$R_{eq,k}$	equivalent resistance for each RL network
t_i	recorded time point
t_1 and t_N	start point and end point of the CV charging process
V_p	voltage across the RC network
V_t	battery terminal voltage
$y_{mea,i}$	measured value
$y_{est,i}$	estimated value
$\overline{y}_{mea}$	mean value of the measured data
τ_{eq}	equivalent time constant
$\tau_{eq,k}$	equivalent time constant for each RL network
θ	vector of unknown model parameters

technique, the battery model is a basic issue for most of the state estimation algorithms. Hence, a simple yet accurate battery model is essential for a high-performance BMS.

1.1. Review of the literature

Due to the relatively simple structure and the satisfactory accuracy, the equivalent circuit model (ECM) is widely used for the on-board battery terminal voltage prediction and state estimation [12]. The conventional ECM consists of a finite number of resistor–capacitor (RC) networks connected in series. Specifically, the RC network is used to describe the polarization effects, and a higher number of RC networks (i.e., a higher order ECM) yields a higher degree of battery terminal voltage estimation accuracy [13,14]. However, at the same time, the complex model increases the computational burden and reduces the numerical stability for the subsequent battery state estimation, which limits its application on the low-cost microcontroller [15,16]. Different ECMs of lithium-ion batteries have been compared and analyzed in the literature by many authors. For example, Ref. [17] conducted a comparative study of twelve ECMs in terms of the model complexity, accuracy and robustness. Ref. [14] compared and analyzed seven impedance-based ECMs with respect to their voltage estimation and state-of-available-power prediction accuracy. Ref. [18] provided a comprehensive overview of the available battery/supercapacitor models, with a particular focus on fractional-order techniques. Besides, in order to decrease the computational effort without sacrificing the model accuracy, Ref. [19] simplified the complex ECM into the type of reduced order based on the dynamics of the battery. Additionally, a measurement noise model and data rejection were implemented to ensure the subsequent SoC estimation accuracy. Ref. [20] proposed an adaptive battery model based on a remapped variant of the Randles' circuit model, and the subspace parameter-estimation algorithms were applied online and in combination with the battery state estimation. Experimental results demonstrated the superiority of this model to the conventional Randles' circuit, in terms of the parameter identification and the states estimation performances. Ref. [21] developed an accurate battery model by considering the hysteresis dependence in the relationship between the open circuit voltage (OCV) and SoC, which ensured an accurate and stable SoC estimation. Ref. [22] employed the 1st-order ECM to estimate the battery SoC, and updated the model parameters online through the extended Kalman filter. Moreover, to reduce the convergence time, the initial states were determined by the recursive least squares algorithm and the off-line identification method.

It has to be noted that the ECMs within the aforementioned study are mainly used to predict the battery voltage response in the vehicle driving condition. For EVs, due to the dynamic and uncertain driving profile, the discharging process of the on-board battery tends to be incomplete and within a random SoC range. Hence, it is a challenging task to precisely evaluate the battery aging state, especially the capacity degradation, based on the driving profile [23]. However, it is more convenient for the BMS to estimate the battery SoH based on the relatively simple charging profile, such as the constant-current constant-voltage (CCCV) charging profile [24–26]. Abundant researches have been conducted to seek the accurate model for the battery under the CC charging condition. Tsang et al. [27] used a universal battery model based on a simple mathematical equation to capture the charging characteristics of the battery. The least squares algorithm was utilized to obtain the unknown model parameters. Verification results demonstrated that this model can capture the charging profiles at different charging rates. Furthermore, Low et al. [28] considered the influence of various ambient temperatures on this model, and developed a new temperature-based equation to represent the normalized CC charging profile at various ambient temperatures. Alfi. et al. [7] trained the radial basis function network offline with the data collected from the battery charging process, then this kind of neural network was applied to determine the battery SoC. Compared with the constant-current (CC) profile, the constant-voltage (CV) profile is more robust to the uncertain initial charging state. In addition, the loss of lithium inventory occurred during the CV profile is more common and obvious than that occurred during the CC profile. Ning et al. [29] verified that 5.5% of the cyclable lithium loss took place in the CC charge mode but 94.5% cyclable lithium loss took place in the CV charge mode. These results confirmed that the measurements during the CV charging profile is effective to reflect the battery aging state. In order to quantitatively describe the dynamic characteristic of the current during the CV charging period, Eddahech et al. [30] used a simple exponential function based mathematical model to simulate the corresponding current behavior. In addition, they found that one of the identified model parameters was closely related to the battery capacity loss, and demonstrated a linear function with respect to the SoH. Yang et al. [31] and Wang et al. [32] obtained the detailed expression of the CV charging current based on the conventional first-order ECM, thus the associated parameters had the explicit physical meaning. Besides, two current-related characteristic parameters, i.e., the current time constant and the CV charging

aging factor, respectively, were further extracted to indicate the battery SoH. Although the estimated current in [31] can overall track the measured value, obvious mismatches were still observed at the initial and end regimes of the CV charging period.

1.2. Contributions of the paper

The objective of this manuscript is to seek a practical ECM that allows for accurate estimation of battery current under the CV charging condition. The main contributions of this paper are:

(1) A resistor-inductor (RL) network-based ECM is first introduced. The mathematical expression of the CV charging current is derived based on the conventional RC network-based ECM. According to the analysis of the expression, a novel ECM containing the RL network is proposed to characterize the battery current behavior though the CV charging period.
(2) Enhanced ECMs consisting of multiple RL networks are developed. Considering the nonlinear characteristic of the CV charging current, a higher order ECM with multiple RL networks connected in parallel are proposed to capture the current characteristic more precisely.
(3) A comparative study is conducted to determine the preferred model structure. The test data of four lithium iron phosphate ($LiFePO_4$) batteries after different aging cycles are employed to validate the feasibility and superiority of the developed model. Comparative results demonstrate that the proposed 2nd-order ECM is the best choice, considering both the model accuracy and complexity.
(4) The simplified model is further developed. By analyzing the identified parameters of the 2nd-order ECM, a simplified model is proposed with satisfactory current estimation accuracy while with less parameterization effort in comparison to the same order ECM.

1.3. Organization of the paper

The reminder of this paper is organized as follows: In Section 2, the novel RL network-based ECM is introduced to characterize the CV charging current. In Section 3, the test procedure including the characterization tests and the aging tests are conducted based on four $LiFePO_4$ batteries. In Section 4, the model parameterization method is presented, and the experimental results are performed to evaluate the performance of the proposed model. In Section 5, a simplified model is developed with satisfactory current estimation accuracy and less parameterization effort. Finally, some conclusions, the advantages of the proposed model, and the future work are given in Section 6.

2. Model development

2.1. RC network-based equivalent circuit model

The conventional ECM is mainly based on the RC network. Take the first-order ECM as an example, it is generally comprised of a voltage source V_{oc}, an Ohmic resistance R_o and a RC network, which contains a resistance R_p and a capacitance C_p connected in parallel, as shown in Fig. 1.

Based on the Kirchoff's law, the electrical behavior of the first-order ECM can be expressed as

$$C_p\frac{dV_p}{dt}+\frac{V_p}{R_p}=I \tag{1}$$

$$V_{OC}+R_oI+V_p=V_t \tag{2}$$

where V_t denotes the battery terminal voltage, V_p denotes the overvoltage across the RC network, and I denotes the load current (the positive value represents charging and the negative value represents discharging).

The battery terminal voltage is set as constant in the CV charging mode, while the charging current decreases continuously with time. In order to quantitatively describe the dynamic characteristic of the CV charging current, it is essential to derive the mathematical expression of the current in the CV mode. By substituting (2) into (1), the differential equation is rewritten as

$$C_p\frac{d(V_t-V_{OC}-R_oI)}{dt}+\frac{V_t-V_{OC}-R_oI}{R_p}=I \tag{3}$$

where V_{OC} denotes the open circuit voltage, and can be represented as a function of SoC, i.e.:

$$\mathrm{OCV}=\mathrm{f(SoC)} \tag{4}$$

where SoC can be further expressed as

$$SoC(t_i)=\mathrm{SoC}(0)+\frac{\eta\int_0^{t_i}\mathrm{I(t)dt}}{3600\mathrm{C_{cap}}} \tag{5}$$

where SoC(t_i) is the SoC at time t_i, SoC(0) is the SoC at initial time, $I(t)$ denotes the current at time t, C_{cap} denotes the battery capacity in Ah, η denotes the coulombic efficiency, and $\eta\approx 1$ [11,33].

Based on (4) and (5), the variation of OCV with respect to time can be expressed as

$$\frac{d\mathrm{OCV}}{dt}=\frac{d\mathrm{OCV}}{d\mathrm{SoC}}\cdot\frac{d\mathrm{SoC}}{dt}=\frac{d\mathrm{OCV}}{d\mathrm{SoC}}\cdot\frac{\eta I(t)}{3600C_{cap}} \tag{6}$$

where $I(t)$ is usually lower than C/2 during the CV charging process, which means that the value of $\eta I(t)/(3600C_{cap})$ is generally less than 0.000139 in the CV mode. Hence, the value of $d\mathrm{SoC}/dt$ is very small, and $d\mathrm{OCV}/dt\approx 0$ holds for the CV charging process.

Similarly, the variation of the impedance parameter can be considered negligible in the CV charging mode, i.e., $dR_p/dt\approx 0$. In addition, $dV_t/dt=0$ can be obtained since the battery terminal voltage during the CV period is controlled constant.

Based on the aforementioned analysis, Eq. (3) can be simplified as

$$\frac{dI}{dt}+\frac{R_o+R_p}{R_oR_pC_p}I=\frac{V_t-V_{OC}}{R_oR_pC_p} \tag{7}$$

Assuming that V_t, V_{oc} and the impedance parameters (i.e., R_o, R_p and C_p) are all known variables, the detailed expression of the CV charging current can be solved as

$$I(t)=I(0)e^{-\frac{(R_o+R_p)t}{R_oR_pC_p}}+\frac{V_t-V_{OC}}{R_o+R_p}\left[1-e^{-\frac{(R_o+R_p)t}{R_oR_pC_p}}\right] \tag{8}$$

where $I(0)$ denotes the current at the beginning of the CV mode.

Defining $R_o+R_p=a$ and $(R_oR_pC_p)/(R_o+R_p)=b$, Eq. (8) can be simplified as

$$I(t)=I(0)e^{-\frac{t}{b}}+\frac{V_t-V_{OC}}{a}\left(1-e^{-\frac{t}{b}}\right) \tag{9}$$

2.2. The proposed equivalent circuit model for CV charging mode

For the system represented by (9), defining (V_t-V_{oc}) as the system

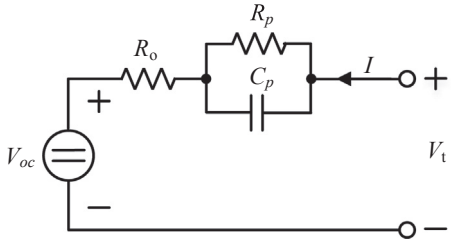

Fig. 1. The first-order ECM.

input and I as the system output, Eq. (9) can be considered as the sum of the zero input response $y_1 = I(0)e^{-t/b}$ and the zero state response $y_2 = (V_t - V_{oc})(1 - e^{-t/b})/a$. For the zero input response y_1, the value decreases exponentially to zero with time. For the zero state response y_2, the value increases exponentially from zero to the steady state $(V_t - V_{oc})/a$. It can be concluded from (9) that the variation rates of y_1 and y_2 are dependent on b, which can be considered as the time constant of the system. Based on the above analysis, Eq. (9) can be represented by an ECM containing one RL network, as shown in Fig. 2.

The electrical behavior of the proposed ECM can be expressed as

$$V_{OC} + R_{eq}I + L_{eq}\frac{dI}{dt} = V_t \tag{10}$$

where R_{eq} is the equivalent resistance and L_{eq} is the equivalent inductance.

Based on the discussion in Section 2.1, $dV_{oc}/dt \approx 0$ holds for the CV charging mode, thus I can be solved as

$$I(t) = I(0)e^{-\frac{t}{\tau_{eq}}} + \frac{V_t - V_{OC}}{R_{eq}}\left(1 - e^{-\frac{t}{\tau_{eq}}}\right) \tag{11}$$

where τ_{eq} is the equivalent time constant and $\tau_{eq} = L_{eq}/R_{eq}$.

By comparing (11) and (9), it is clear that the two equations have the same form when satisfying $a = R_{eq}$ and $b = \tau_{eq}$, proving the effectiveness of the proposed model structure. In addition, it can be concluded that the proposed ECM shown in Fig. 2 contains less components compared with the conventional one shown in Fig. 1, which in turn leads to a lower parameterization effort.

For the CV charging mode, the battery terminal voltage remains constant, while the load current decays nonlinearly with time, causing the concentration gradient of lithium ions to decrease progressively to a slight level when the CV charge ends [29,30]. Hence, the CV charging current is closely related to the nonlinear electrochemical processes occurred inside the battery. It can be concluded form (11) that the dynamic characteristic of the CV charging current is mainly determined by the time constant of the RL network. However, the estimated current obtained based on the ECM shown in Fig. 2 cannot closely track the measured value, which will be discussed in Section 4.2. In the conventional ECM, the RC network is widely adopted to approximate the nonlinear polarization effects in the time domain, and a higher number of RC networks with different time constants are generally connected in series to give a better approximation [34]. Hence, in order to accurately describe the dynamic characteristic of the CV charging current, exponential functions with different time constants are employed together to reproduce the battery electrochemical processes. Correspondingly, the proposed ECM shown in Fig. 2 can be extended to a higher order with multiple RL networks connected in parallel, as shown in Fig. 3.

For the ECM shown in Fig. 3, the equation of the branch current through each RL network are similar to (11). In addition, according to Kirchoff's current law, the sum of branch currents flowing into the node, i.e., point A in Fig. 3, is equal to the value of the total charging current. Hence, the detailed expressions of each branch current and the associated relationships are

$$\begin{cases} I_k(t) = I_k(0)e^{-\frac{t}{\tau_{eq,k}}} + \frac{V_t - V_{OC}}{R_{eq,k}}(1 - e^{-\frac{t}{\tau_{eq,k}}}), & k = 1, 2, ...,n \\ \sum_{k=1}^{n} I_k(t) = I(t) \end{cases} \tag{12}$$

where n is the order of the model, $I_k(t)$ denotes the branch current through each RL network, $R_{eq,k}$ and $\tau_{eq,k}$ denote the equivalent resistance and the equivalent time constant for each RL network, respectively.

3. Experimental tests

3.1. Experimental setup

The batteries employed in this study are four 26,650 power cells, which are numbered from #1 to #4. Four batteries are stimulated with the same load current or power profiles for comparison and validation. The key specifications of the investigated battery are listed in Table 1.

The tests are conducted on an 8-channel Arbin BT2000 battery cycler with a voltage range of 0–5 V and a current range of −100 to 100 A. The voltage and current accuracy is ± 0.02% for low power and ± 0.05% for high power applications. All four batteries are placed in an air-conditioned room with a temperature range of 25 ± 2 °C, and the sampling frequency of the data acquisition is set as 1 Hz.

3.2. Test procedure

The battery test procedure consists of two parts, i.e., the characterization tests and the aging test. The objective of the characterization tests is to obtain the batteries' capacity and SoC-OCV correlation, so as to identify the impedance parameters of the ECM derived in Section 2.2. The aging test is utilized to cycle the investigated batteries to different aging states.

3.2.1. Characterization tests

In order to extract the battery information at different aging states, the characterization tests are conducted after a certain number of aging tests. The characterization tests in this study are composed of two parts: the capacity test and the hybrid pulse power characterization (HPPC) test.

The capacity test includes 5 charge-discharge cycles. In each cycle, the battery is first charged at a constant current of 0.5C rate until the battery terminal voltage reaches the cut-off value of 3.65 V, then a CV mode is applied until the charging current reaches the cut-off value of C/20. After resting for 1 h, the battery is discharged in a CC mode at 0.5C rate until the battery terminal voltage reaches 2.0 V. The rest period between two cycles is 1 h. Finally, the battery's capacity is calculated as the mean value of the accumulative charge of 5 cycles.

It can be inferred from (12) that the input variable of the system contains the battery OCV, which should be determined in advance. In this study, the SoC-OCV correlation is obtained by the HPPC test. In the HPPC test, the battery is first stimulated with a pair of discharge and charge current pulses, with the amplitude of 2C and the duration of 10 s. Then, after resting for 60 s, the battery is incrementally discharged/charged with the interval of 5% SoC at a constant current of 0.5C rate, this is followed by a 2 h relaxation period to reduce the polarization effects.

3.2.2. Aging tests

After the characterization tests, the investigated batteries are cycled in the aging test. In each aging cycle, all four batteries are charged at a constant current of 1C rate until the charge cut-off voltage (3.65 V) is reached, then the CV charging mode is conducted until the current reduces to C/20. After that, the batteries are discharged immediately in a CC mode at 4C rate to the discharge cut-off voltage (2.0 V).

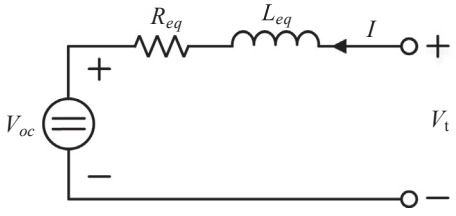

Fig. 2. Proposed RL network-based ECM.

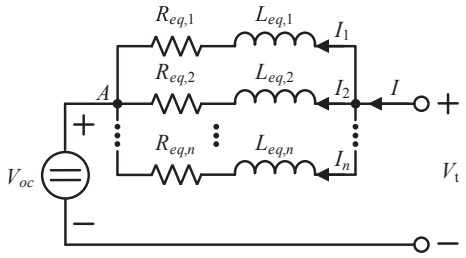

Fig. 3. Proposed n^{th}-order ECM.

Table 1
Specifications of investigated batteries.

Chemistry	$LiFePO_4$
Nominal capacity (at C/5 rate)	2.5 Ah
Nominal voltage	3.2 V
Charge cut-off voltage	3.65 V
Discharge cut-off voltage	2.0 V

4. Model parameterization and verification

4.1. Model parameterization

The time-current series acquired during the CV charging period are employed to identify the model parameters. In this study, all the time-current series are extracted from the 5th cycle in the capacity test. Specifically, the time-current series can be denoted as $\{(t_i, I_{mea,i}), i = 1, 2, \ldots, N\}$, where t_i is the recorded time point, $I_{mea,i}$ is the measured current value at t_i, and N is the recorded data size. t_1 and t_N correspond to the start point and the end point of the CV charging process, respectively, and $t_1 = 0$.

The nonlinear least squares (NLS) algorithm is employed to fit the measured time-current series, and the model parameters can be obtained by solving the cost function as [35,36]

$$J = \arg\min\left[\sum_{i=1}^{N}(\mathrm{I_{mea,i}(t_i)} - \mathrm{I_{est,i}(t_i,\theta)})^2\right] \tag{13}$$

where $I_{est,i}$ denotes the estimated current, θ denotes the vector of unknown model parameters, and $\theta = [R_{eq,1}\ldots R_{eq,n}, L_{eq,1}\ldots L_{eq,n}, I_2(0)\ldots I_n(0)]$.

4.2. Model verification

In order to verify the feasibility of the proposed ECM and investigate the influence of the number of the RL networks on the current estimation accuracy, the CV data of battery #1 are used for the parameter identification and the CV data of other batteries are used for the model verification. Fig. 4 demonstrates the estimation results and the absolute values of errors for battery #2 at different aging states (i.e., new, 150 cycles, 900 cycles and 2050 cycles). It is worth noting that the current generated by the proposed 1st-order ECM is equal to that estimated by the conventional 1st-order RC network-based ECM. In this study, the ECMs containing more than 3 RL networks are not considered due to the high parameterization effort. The obvious fluctuations are observed in the obtained estimation errors, as shown in Fig. 4(b), (d), (f) and (h), which are mostly due to the measurement noise. Besides, it can be seen from Fig. 4 that the estimation results based on the proposed ECMs can generally track the measured current at different aging states. Moreover, the current estimation accuracy is improved significantly from the proposed 1st-order ECM (or the conventional 1st-order RC network-based ECM) to the 2nd-order ECM. However, the error curves of the 2nd-order ECM and the 3rd-order ECM are almost overlapped with each other. This indicates that no obvious improvement is observed from the 2nd-order model to the 3rd-order model.

In order to quantitatively assess the estimation results of the proposed ECMs, two evaluation criterions, including the root mean-squared error (RMSE) and the R-square (R^2), are calculated as

$$\mathrm{RMSE} = \sqrt{\frac{1}{\mathrm{N}}\sum_{\mathrm{i=1}}^{\mathrm{N}}(\mathrm{y_{mea,i}} - \mathrm{y_{est,i}})^2} \tag{14}$$

$$\mathrm{R^2} = 1 - \frac{\sum_{\mathrm{i=1}}^{\mathrm{N}}(\mathrm{y_{mea,i}} - \mathrm{y_{est,i}})^2}{\sum_{\mathrm{i=1}}^{\mathrm{N}}(\mathrm{y_{mea,i}} - \bar{\mathrm{y}}_{\mathrm{mea}})^2}, \quad \bar{\mathrm{y}}_{\mathrm{mea}} = \frac{1}{\mathrm{N}}\sum_{\mathrm{i=1}}^{\mathrm{N}}\mathrm{y_{mea,i}} \tag{15}$$

where N denotes the data size, $y_{mea,i}$ and $y_{est,i}$ denote the measured and the estimated values, respectively, $\bar{y}_{mea}$ denotes the mean value of the measured data. Specifically, a lower RMSE (closer to 0) and a larger R^2 (closer to 1) indicate a more accurate estimation result.

Fig. 5 demonstrates the calculated evaluation criterions of the model current estimation for battery #2 at different aging states. The obvious reduction of RMSE and increase of R^2 are observed from the 1st-order ECM to the 2nd-order ECM. By contrast, the variations of the evaluation criterions are much smaller from the 2nd-order ECM to the 3rd-order ECM. These phenomena are in accordance with the estimation results depicted in Fig. 4. In addition, it can be seen from Fig. 5(b) that both the R^2s of the 2nd-order ECM and the 3rd-order ECM are close to 1, indicating the high current estimation accuracy of these two models.

In order to further verify the applicability of the proposed model, the obtained RMSE and R^2 of battery #2, #3 and #4 are listed in Table 2. As can be seen, the aging states of all three batteries have no significant influence on the estimation accuracy of the proposed ECMs. In addition, the parameters identified from one battery (battery #1) can be applied to estimate the charging current of other three batteries with satisfactory performance. Besides, it can be found from Table 2 that the model accuracy is closely related to the model structure. Take battery #2 as an example, for the 2nd-order model, the RMSE is reduced by approximately 75.4% overall and with 3 more model parameters in comparison to the 1st-oder model. Moreover, the overall RMSE is only reduced by approximately 10.5% from the 2nd-oder model to the 3rd-order model, but the model parameters are increased from 5 to 8. This phenomenon can also be verified by the estimation results of battery #3 and battery #4. It can be concluded that the higher number of RL networks leads to the better current estimation performance; however, at the expense of the higher parameterization effort. Hence, considering the tradeoff between the model fidelity and the parameterization effort, the proposed 2nd-order ECM is the best choice to characterize the CV charging current.

On the other hand, the mathematical function proposed in Ref. [30] is also conducted to make a comparison. Specifically, the mathematical function is expressed as

$$I(\mathrm{t}) = \mathrm{Ae^{-Bt}} + \mathrm{C} \tag{16}$$

where A, B and C are the function coefficients, which can be identified by the NLS algorithm described in Section 4.1.

Table 3 shows the calculated evaluation criterions of the current estimation results by (16). By comparing Tables 2 and 3, it demonstrates that for all three tested batteries, the proposed ECM containing more than one RL network can provide more accurate estimated current, which further proves the superiority of the proposed ECM in terms of the estimation accuracy.

5. Model simplification

Based on the aforementioned analysis, it can be concluded that the proposed ECM containing 2 RL networks can ensure the sufficient accuracy of current estimation. Table 4 gives the identified model parameters for battery #1 at different aging states.

According to (12), it is clear that the values of $(V_t - V_{oc})$ and $R_{eq,k}$

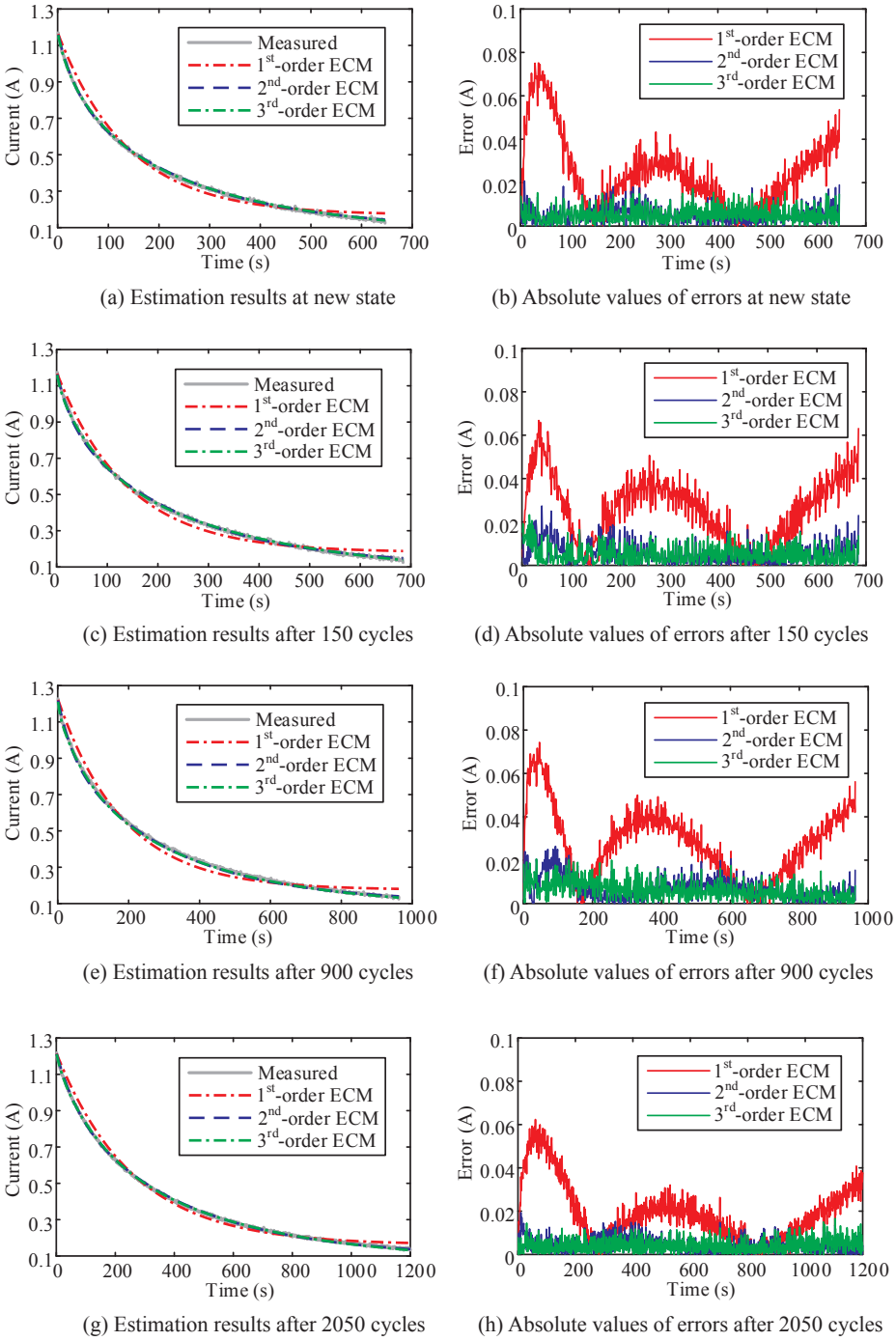

(a) Estimation results at new state (b) Absolute values of errors at new state

(c) Estimation results after 150 cycles (d) Absolute values of errors after 150 cycles

(e) Estimation results after 900 cycles (f) Absolute values of errors after 900 cycles

(g) Estimation results after 2050 cycles (h) Absolute values of errors after 2050 cycles

Fig. 4. Current estimation results and absolute values of errors for the proposed ECMs.

directly influence the zero state current response. The value of V_{oc} is generally close to the battery terminal voltage during the CV charging mode, leading to a low $(V_t - V_{oc})$ value (approximate 0.296 V). It can be observed from Table 4 that the estimated equivalent resistances, especially $R_{eq,2}$, possess relative high values. Hence, the $(V_t - V_{oc})(1 - e^{-t/\tau eq,k})/R_{eq,k}$ ($k = 1$ and 2) part in the estimated current can be neglected, which means that the fitting function of the 2nd-order ECM can be simplified as

$$I(t) = I_1(0)e^{-\frac{t}{\tau_{eq,1}}} + [I(0) - I_1(0)]e^{-\frac{t}{\tau_{eq,2}}} \quad (17)$$

It can be found from (17) that only three model parameters are required to be identified, i.e., $I_1(0)$, $\tau_{eq,1}$ and $\tau_{eq,2}$.

In order to assess the performance of the simplified model, Fig. 6 shows the estimation results and the absolute values of errors at different aging states. Specifically, the model parameters are identified based on the test data of battery #1, and the estimation results based on the test data of battery #2 are demonstrated as examples. In addition, the evaluating criterions of battery #2, #3 and #4 are listed in Table 5. As can be seen, the estimated current curve matches well with the measured results at different battery aging states. By comparing Tables 2 and 5, it can be observed that the current estimation accuracy is slightly decreased from the 2nd-order model to the respective simplified one, due to the neglect of the $(V_t - V_{oc})(1 - e^{-t/\tau eq,k})/R_{eq,k}$ ($k = 1$ and 2) part. Compared with the 1st-order model, the estimation accuracy of the simplified model is significantly improved with the same number of model parameters. Hence, it can be concluded that for the

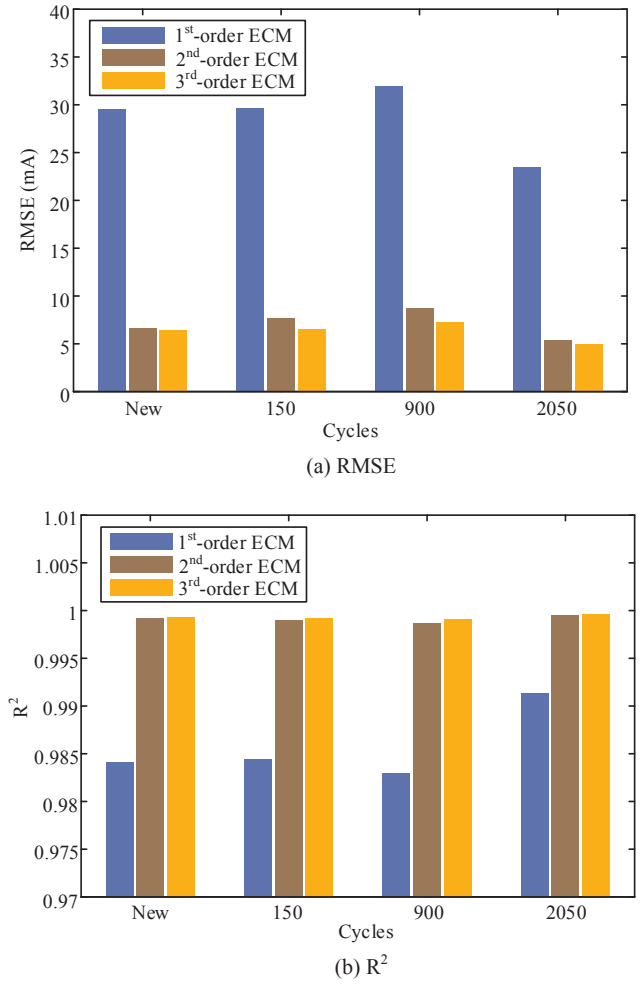

Fig. 5. Quantitative assessment of model current estimation at different aging states.

simplified 2nd-order model, the number of model parameters is reduced, yet the current estimation accuracy can still be guaranteed.

6. Conclusion

A novel RL network-based ECM is proposed in this paper, which can capture the dynamic characteristic of the charging current at CV mode. According to the current expression derived upon the conventional RC network-based ECM, a battery ECM containing one RL network is first introduced. Secondly, in order to improve the model fidelity, the proposed model is generalized to a higher order with multiple RL networks connected in parallel with each other. Thirdly, based on the analysis of the identified model parameters, a simplified 2nd-order model is developed to decrease the parameterization effort. Lastly, the NLS algorithm is employed to identify the model parameters, and four $LiFePO_4$ batteries are tested to validate the proposed model. Comparison results indicate that a higher number of RL networks lead to a more accurate current estimation, however, at the expense of higher parameterization effort. Besides, the simplified 2nd-order model can be a good candidate considering the tradeoff between the model accuracy and complexity.

The proposed model has several advantages desired for the BMS. First, it contains less parameters compared to the conventional RC network-based ECM with the same order, and thus requires a lower parameterization effort. For the simplified model, this superiority is enhanced since the number of identified model parameters is further reduced. In addition, due to the electrical characteristic of the RL network, the proposed model can capture the dynamics of the CV charging current precisely. According to our previous work [31], the dynamic characteristic of the charging current during the CV period is closely related to the battery aging state. Hence, with the proposed model, it is possible to explore an effective way to estimate the battery SoH.

In this paper, only $LiFePO_4$ batteries are adopted in the test, and the test temperature is maintained around 25℃. Hence, future work will be focused on verifying the proposed model with different battery chemistries at different temperatures. In addition, a novel battery SoH estimation method based on the developed model will be presented.

Table 3
Calculated evaluation criterions of the current estimation results by (16).

Battery Number	New		150 Cycles		900 Cycles		2050 Cycles	
	RMSE (mA)	R^2	RMSE (mA)	R^2	RMSE (mA)	R^2	RMSE (mA)	R^2
#2	18.3	0.9939	18.4	0.9940	17.9	0.9946	14.2	0.9968
#3	19.1	0.9935	18.7	0.9938	18.9	0.9941	19.2	0.9941
#4	19.2	0.9934	19.7	0.9932	18.8	0.9941	14.8	0.9966

Table 4
Identified model parameters for battery #1.

	New	150 cycles	900 cycles	2050 cycles
$\tau_{eq,1}$ (s)	35.0047	29.4680	41.0657	71.1882
$R_{eq,1}$ (Ω)	3.1164	2.7898	2.6872	3.0705
$\tau_{eq,2}$ (s)	237.2236	235.9098	300.3323	401.5255
$R_{eq,2}$ (Ω)	1.4043×10^3	1.6499×10^3	1.8870×10^3	2.4041×10^3
$I_2(0)$ (A)	0.7854	0.8169	0.8381	0.8530

Acknowledgements

The authors would like to acknowledge the funding support from

Table 2
Calculated evaluation criterions of the current estimation results by the proposed ECMs.

Battery Number	Model Structure	New		150 Cycles		900 Cycles		2050 Cycles	
		RMSE(mA)	R^2	RMSE(mA)	R^2	RMSE(mA)	R^2	RMSE(mA)	R^2
#2	1st-order	29.6	0.9841	29.7	0.9844	32.0	0.9829	23.5	0.9913
	2nd-order	6.6	0.9992	7.7	0.9990	8.7	0.9987	5.4	0.9995
	3rd-order	6.4	0.9993	6.5	0.9992	7.3	0.9991	5.0	0.9996
#3	1st-order	38.2	0.9741	31.5	0.9825	31.7	0.9833	27.1	0.9883
	2nd-order	9.0	0.9985	8.7	0.9987	11.5	0.9978	13.0	0.9973
	3rd-order	6.9	0.9992	7.4	0.9990	10.3	0.9982	12.9	0.9973
#4	1st-order	29.6	0.9843	35.2	0.9783	31.5	0.9834	22.6	0.9920
	2nd-order	10.0	0.9982	10.1	0.9982	11.3	0.9979	7.6	0.9991
	3rd-order	9.7	0.9983	9.2	0.9985	10.1	0.9983	6.8	0.9993

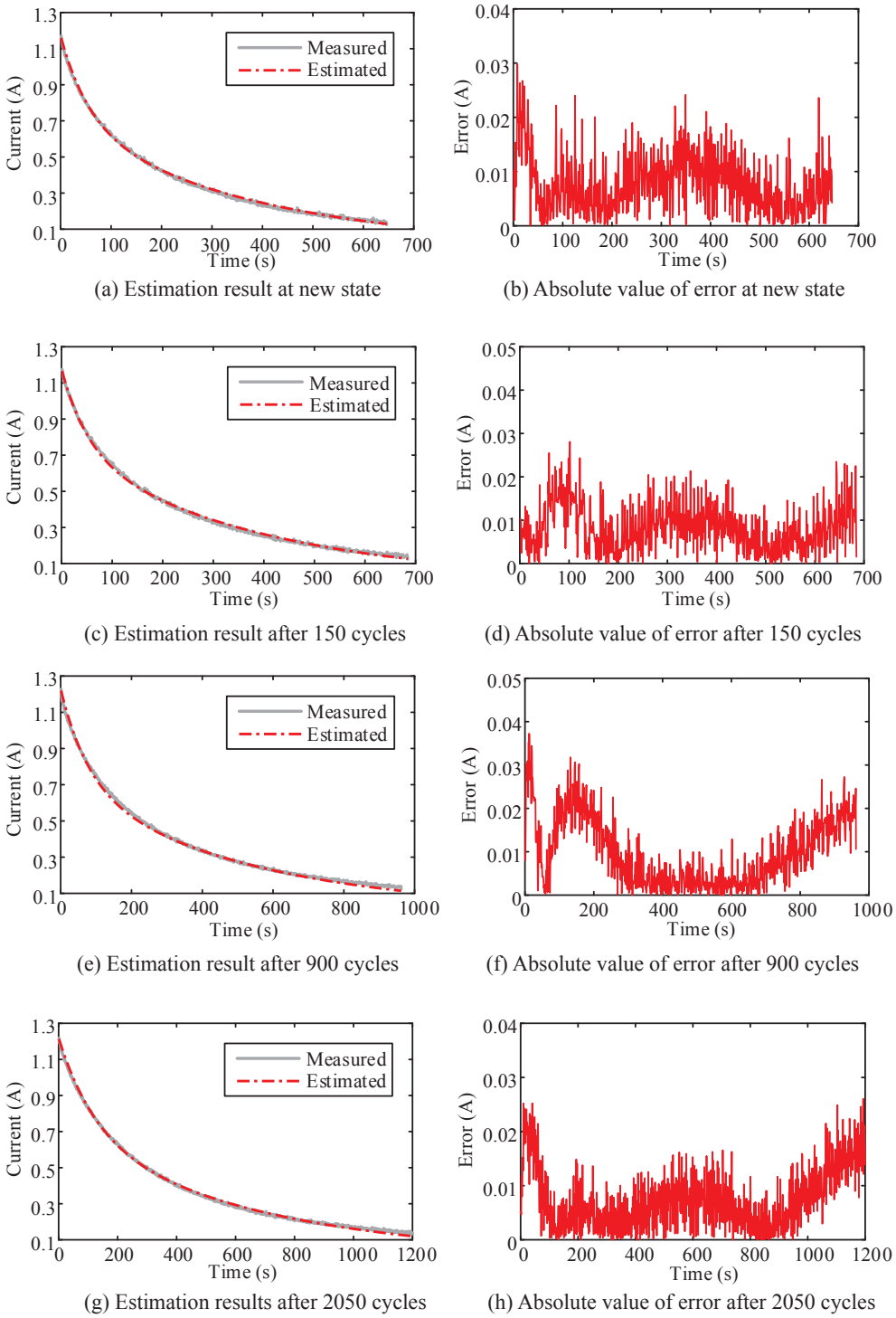

Fig. 6. Current estimation results and absolute values of errors for the proposed simplified model.

Table 5
Calculated evaluation criterions of the proposed simplified model.

Battery Number	New		150 cycles		900 cycles		2050 cycles	
	RMSE (mA)	R^2	RMSE (mA)	R^2	RMSE (mA)	R^2	RMSE (mA)	R^2
#2	9.4	0.9984	9.9	0.9983	12.4	0.9975	9.2	0.9987
#3	13.7	0.9967	11.5	0.9977	15.0	0.9962	15.1	0.9964
#4	11.6	0.9976	13.1	0.9970	14.6	0.9964	9.1	0.9987

the National Science Foundation, US (1507198); the National Natural Science Foundation of China (51875255, U1664258); and the Natural Science Foundation of Jiangsu Province (BK20171300).

References

[1] Zhang X, Mi C. Vehicle power management: modeling, control and optimization. Springer Science & Business Media; 2011.
[2] Nasri A, Abdollahi A, Rashidinejad M, Amini MH. Probabilistic–possibilistic model for a parking lot in the smart distribution network expansion planning. IET Gener Transm Distrib 2018;12:3363–74.
[3] Cai Y, Wang H, Zheng Z, Sun X. Scene-adaptive vehicle detection algorithm based

on a composite deep structure. IEEE Access 2017;5:22804–11.
[4] M. H. Amini, A Panorama of Interdependent Power Systems and Electrified Transportation Networks, 2019.
[5] Lu L, Han X, Li J, Hua J, Ouyang M. A review on the key issues for lithium-ion battery management in electric vehicles. J Power Sources 2013;226:272–88.
[6] Yang X, Chen L, Xu X, Wang W, Xu Q, Lin Y, et al. Parameter identification of electrochemical model for vehicular lithium-ion battery based on particle swarm optimization. Energies 2017;10:1811.
[7] Alfi A, Charkhgard M, Zarif MH. Hybrid state of charge estimation for lithium-ion batteries: design and implementation. IET Power Electron 2014;7:2758–64.
[8] Wang L, Lu D, Liu Q, Liu L, Zhao X. State of charge estimation for LiFePO4 battery via dual extended kalman filter and charging voltage curve. Electrochim Acta 2019;296:1009–17.
[9] Williard N, He W, Osterman M, Pecht M. Comparative analysis of features for determining state of health in lithium-ion batteries. Int J Progn Health Manage 2013;4.
[10] Wang L, Pan C, Liu L, Cheng Y, Zhao X. On-board state of health estimation of LiFePO4 battery pack through differential voltage analysis. Appl Energy 2016;168:465–72.
[11] Wang Y, Zhang C, Chen Z. A method for joint estimation of state-of-charge and available energy of LiFePO4 batteries. Appl Energy 2014;135:81–7.
[12] Hariharan KS, Senthil Kumar V. A nonlinear equivalent circuit model for lithium ion cells. J Power Sources 2013;222:210–7.
[13] He H, Xiong R, Guo H, Li S. Comparison study on the battery models used for the energy management of batteries in electric vehicles. Energy Convers Manage 2012;64:113–21.
[14] Farmann A, Sauer DU. Comparative study of reduced order equivalent circuit models for on-board state-of-available-power prediction of lithium-ion batteries in electric vehicles. Appl Energy 2018;225:1102–22.
[15] Zou Y, Hu X, Ma H, Li SE. Combined state of charge and state of health estimation over lithium-ion battery cell cycle lifespan for electric vehicles. J Power Sources 2015;273:793–803.
[16] Yang J, Huang W, Xia B, Mi C. The improved open-circuit voltage characterization test using active polarization voltage reduction method. Appl Energy 2019;237:682–94.
[17] Hu X, Li S, Peng H. A comparative study of equivalent circuit models for Li-ion batteries. J Power Sources 2012;198:359–67.
[18] Zou C, Zhang L, Hu X, Wang Z, Wik T, Pecht M. A review of fractional-order techniques applied to lithium-ion batteries, lead-acid batteries, and supercapacitors. J Power Sources 2018;390:286–96.
[19] Lee J, Nam O, Cho BH. Li-ion battery SOC estimation method based on the reduced order extended Kalman filtering. J Power Sources 2007;174:9–15.
[20] Gould CR, Bingham CM, Stone DA, Bentley P. New battery model and state-of-health determination through subspace parameter estimation and state-observer techniques. IEEE Trans Veh Technol 2009;58:3905–16.
[21] Pérez G, Garmendia M, Reynaud JF, Crego J, Viscarret U. Enhanced closed loop state of charge estimator for lithium-ion batteries based on extended Kalman filter. Appl Energy 2015;155:834–45.
[22] Wang Y, Liu C, Pan R, Chen Z. Modeling and state-of-charge prediction of lithium-ion battery and ultracapacitor hybrids with a co-estimator. Energy 2017;121:739–50.
[23] Gao W, Zou Y, Sun F, Hu X, Yu Y, Feng S. Data pieces-based parameter identification for lithium-ion battery. J Power Sources 2016;328:174–84.
[24] Andrea D. Battery management systems for large lithium ion battery packs. Artech House 2010.
[25] Deng J, Li S, Hu S, Mi CC, Ma R. Design methodology of LLC resonant converters for electric vehicle battery chargers. IEEE Trans Veh Technol 2014;63:1581–92.
[26] Vu V, Tran D, Choi W. Implementation of the constant current and constant voltage charge of inductive power transfer systems with the double-sided LCC compensation topology for electric vehicle battery charge applications. IEEE Trans Power Electron 2018;33:7398–410.
[27] Tsang KM, Sun L, Chan WL. Identification and modelling of lithium ion battery. Energy Convers Manage 2010;51:2857–62.
[28] Low WY, Aziz MJA, Idris NRN. Modelling of lithium-titanate battery with ambient temperature effect for charger design. IET Power Electron 2016;9:1204–12.
[29] Ning G, White RE, Popov BN. A generalized cycle life model of rechargeable Li-ion batteries. Electrochim Acta 2006;51:2012–22.
[30] Eddahech A, Briat O, Vinassa J-M. Determination of lithium-ion battery state-of-health based on constant-voltage charge phase. J Power Sources 2014;258:218–27.
[31] Yang J, Xia B, Huang W, Fu Y, Mi C. Online state-of-health estimation for lithium-ion batteries using constant-voltage charging current analysis. Appl Energy 2018;212:1589–600.
[32] Wang Z, Zeng S, Guo J, Qin T. State of health estimation of lithium-ion batteries based on the constant voltage charging curve. Energy 2019;167:661–9.
[33] Yang J, Xia B, Shang Y, Huang W, Mi CC. Adaptive state-of-charge estimation based on a split battery model for electric vehicle applications. IEEE Trans Veh Technol 2017;66:10889–98.
[34] Li J, Mazzola MS. Accurate battery pack modeling for automotive applications. J Power Sources 2013;237:215–28.
[35] Yang J, Xia B, Shang Y, Huang W, Mi C. Improved battery parameter estimation method considering operating scenarios for HEV/EV Applications. Energies 2017;10:5.
[36] Bruen T, Marco J. Modelling and experimental evaluation of parallel connected lithium ion cells for an electric vehicle battery system. J Power Sources 2016;310:91–101.